International Journal of Refrigeration 146 (2023) 442–451

Contents lists available at ScienceDirect

International Journal of Refrigeration

journal homepage: www.elsevier.com/locate/ijrefrig

Investigation of refrigerant pipe pressure drop and charge reduction of mobile air conditioning units with R1234yf

Étude de la chute de pression du tuyau de réfrigérant et de la réduction de charge des unités de climatisation mobiles avec R1234yf

Robin Meinert *, Arne Speerforck

Institute of Engineering Thermodynamics, Hamburg University of Technology, Denickestr. 17, 21073 Hamburg, Germany

ARTICLE INFO

Keywords:
Mobile air conditioning
R1234yf
Liquid line
Pressure drop
Charge reduction

Mots clés:
Climatisation mobile
R1234yf
Ligne de liquide
Perte de charge
Réduction de charge

ABSTRACT

In this study, the pressure drop of automotive refrigerant pipes with the refrigerant R1234yf is investigated in detail. For this purpose, 1D and 3D simulations are compared with respect to prediction accuracy using liquid lines from a production car. It is shown that for a combined approach of the methods a very good agreement with the measured values can be obtained, whereas simplified modeling of the line as a straight pipe of equal length significantly underestimates the experimental values. The transition pieces between the pipe and the hose are of particular importance, since they account for up to 85 % of the total pressure drop and therefore result in major errors if neglected. If hoses were eliminated, the lines could be designed smaller, resulting in a charge reduction of up to 56 %.

1. Introduction

Since 2017, the use of refrigerants with a global warming potential (GWP) higher than 150 in air conditioning systems in new vehicles is no longer permitted in the EU (European Union, 2006). This led to the substitution of the widely spread R134a with the low GWP refrigerant R1234yf, which is suitable for direct replacement due to its very similar fluid properties. However, R1234yf has a lower heat of vaporization compared to R134a, requiring a larger mass flow rate to achieve the same cooling capacity (Großmann, 2016). Initial research therefore focused primarily on the change in refrigeration performance and efficiency with a direct drop-in replacement.

Zilio et al. (2011) reported significantly lower cooling capacity and COP. However, with an adjustment of the expansion valve and optimization of the variable displacement compressor valve, the performance could be improved when using R1234yf. Lee and Jung (2012) also conducted experiments on drop-in replacement of R134a by R1234yf. A 4 % lower cooling capacity and a 2.7 % lower COP are found. Navarro-Esbrí et al. (2013) reported larger COP reductions between 5 % to 30 %, comparable values can also be found in Qi (2015), Sánchez et al. (2017) and Sharif et al. (2020). Cho et al. (2013) investigated the system performance of a vehicle refrigeration cycle using R134a and R1234yf. A 7 % lower cooling capacity and a 4.5 % lower COP were described for R1234yf compared to R134a. The use of an internal heat exchanger could reduce the deviation. This effect was also described by Navarro-Esbrí et al. (2013) and Zilio et al. (2009). Pottker and Hrnjak (2015) pointed out that an internal heat exchanger can, however, mitigate efficiency gains from higher condenser subcooling, since both measures compete to reduce throttling losses.

In addition to a large number of experimental studies, several numerical investigations are also available. The drop-in application of R1234yf into a R134a system was simulated by Daviran et al. (2017) in MATLAB. The model included only the main components of the refrigeration cycle, i.e., compressor, condenser, expansion valve, and evaporator. Detailed modeling of the interconnecting piping and other components was omitted. For the same cooling capacity, the COP of the system was calculated to be 1.3 % to 5 % lower than the R134a system by using R1234yf. Devecioğlu and Oruç (2017) compared R444 A and R445 A refrigerants with R1234yf in a theoretical study. The model also included only the compressor, heat exchangers and expansion valve, while the refrigerant lines were neglected. The

* Corresponding author.
E-mail address: robin.meinert@tuhh.de (R. Meinert).

https://doi.org/10.1016/j.ijrefrig.2022.12.005
Received 24 September 2022; Received in revised form 13 November 2022; Accepted 5 December 2022
Available online 8 December 2022

Nomenclature

A_1	Geometry factor (–)
a	Factor (–)
B_1	Geometry factor (–)
d	Diameter (m)
Δp	Pressure drop (bar)
k	Absolute roughness (m)
l	Length (m)
p	Pressure (bar)
r	Bending radius (m)
Re	Reynolds number (–)
T	Temperature (°C)
w	Velocity ($\mathrm{m\,s^{-1}}$)
x	Measured quantity

Greek symbols

δ	Bending angle (°)
η	Dynamic viscosity (Pa s)
ρ	Density ($\mathrm{kg/m^3}$)
ζ	Resistance coefficient (–)

Subscripts

b	Bend
calc	Calculated
i	Inner
meas	Measured
sp	Straight pipe

Abbreviations

COP	Coefficient of performance
GUI	Graphical user interface
GWP	Global warming potential
MRD	Mean relative deviation
PHX	Plate heat exchanger
TP	Transition piece

steady-state observations showed a larger cooling capacity of R444 A and R445 A compared to R1234yf, but a lower COP. This was assigned to a higher electrical power demand. Di Battista and Cipollone (2016) investigated the influence of a liquid cooled condenser on the system efficiency of a R1234yf refrigeration cycle. This was done using a mathematical model which, in addition to the compressor and heat exchangers, consisted of a fixed orifice as an expansion device and a model for the accumulator. There were no connecting lines included in the general model. For the same condensing capacity, a liquid-cooled condenser resulted in a 22 % reduction in compressor power and a 11.8 % increase in evaporator cooling performance. The COP of the system was thus 43.3 % higher than in the system with air-cooled condenser. A second law analysis for a refrigeration cycle with R1234yf was conducted by Golzari et al. (2017) based on a MATLAB model. The exergy dissipation in the main components was determined, but the pressure drop in the connecting lines was neglected. The largest exergy dissipation occurred in the compressor with 53 %, followed by the condenser with 21 %, the expansion valve with 15 %, and the evaporator with 11 %. A comparison with R134a showed greater exergetic efficiency for R1234yf. Huang et al. (2017) investigated the energy-optimized control of a R134a refrigeration cycle based on a dynamic model. In addition to the main components, the interconnecting lines were also modeled, however, only the refrigerant volume was included. The pressure drop was neglected, which was justified by the short tube length. 8 % energy savings were achieved when using a model-based controller compared to a conventional on-off controller. The difference between mechanically and electrically driven compressors in a vehicle air conditioning system was investigated by von Manstein et al. (2017) using a dynamic system model in Modelica. It was shown that electrically driven compressors have efficiency advantages over mechanically driven compressors, especially during engine shut-off phases. The interconnecting lines between the main components were modeled as straight pipes. A comprehensive overview of other research findings on the use of R1234yf in all kinds of HVAC applications is given in Pabon et al. (2020).

Looking at the available literature, it is evident that detailed modeling of refrigerant lines was mostly omitted, often being neglected entirely or only described in a highly simplified way. For the refrigerant CO_2, Subei and Schmitz (2019) investigated the pressure drop of refrigerant pipes in vehicles, both experimentally and numerically. It is found that modeling the lines as a straight pipe of equal length significantly underestimates the pressure drop. Furthermore, the authors showed that one-dimensional and three-dimensional simulation tools do provide more accurate results. However, the pressure drop was also underestimated in this case by up to 25.7 %.

The impact of CO_2 refrigerant pipe pressure drop on system efficiency was studied in Subei (2020). The author identified that the COP of the vehicle refrigeration system is reduced by up to 9.3 % for the case of considering the pipes compared to the case of neglecting them. This appeared particularly for large thermal loads, where high mass flow rates prevail. The results show the large error associated with neglecting the refrigerant pipes.

The design of the lines is always an optimization problem. On the one hand, the inner diameter must not become too small due to excessive pressure drops or efficiency losses, and on the other hand, the inner volume should be kept as small as possible in terms of material and refrigerant costs. In addition to the cost and efficiency variable, there is also an environmental aspect to the refrigerant charge. With a GWP of 4, the refrigerant R1234yf has only a very small global warming potential, which is mainly due to its short atmospheric lifetime of about 11 days (Nielsen et al., 2007). Therefore, released R1234yf decomposes rather quickly, forming aquatic toxic decomposition products (David et al., 2021). Thus, it is necessary to reduce the charge of the refrigeration cycle to minimize the environmental impact. Feng and Hrnjak (2016) analyzed a reversible refrigeration and heat pump system for mobile applications using R134a. In addition to an experimental investigation, numerical simulations were also conducted. A major finding is the large difference in charge volume as soon as the operating mode of the system is changed. The liquid lines, which have large internal volumes, are a major contributor to this. Due to the high density of liquid refrigerant, there is a correspondingly high refrigerant mass in this type of line.

The aim of this paper is to investigate vehicle refrigerant pipes in terms of pressure drop and refrigerant charge. The focus is on liquid lines because, as mentioned earlier, they contain the largest refrigerant mass of all line types. The exact knowledge about the composition of the pressure drop fractions of the line elements can help to improve the accuracy of system models and to be able to size the pipes smaller in order to save refrigerant, weight, installation space and costs. For the study, 1D and 3D numerical simulations are conducted in addition to experiments. It should be noted that the investigation is carried out without considering the impact of oil. For related studies, it is referred to the papers of Sethi and Hrnjak (2014), as well as Xu and Hrnjak (2018).

2. Experimental setup

For the experimental investigation, a test rig designed for the refrigerant R1234yf was planned and constructed. The aim of this facility is to set a defined flow condition at the inlet of a test section. This state is

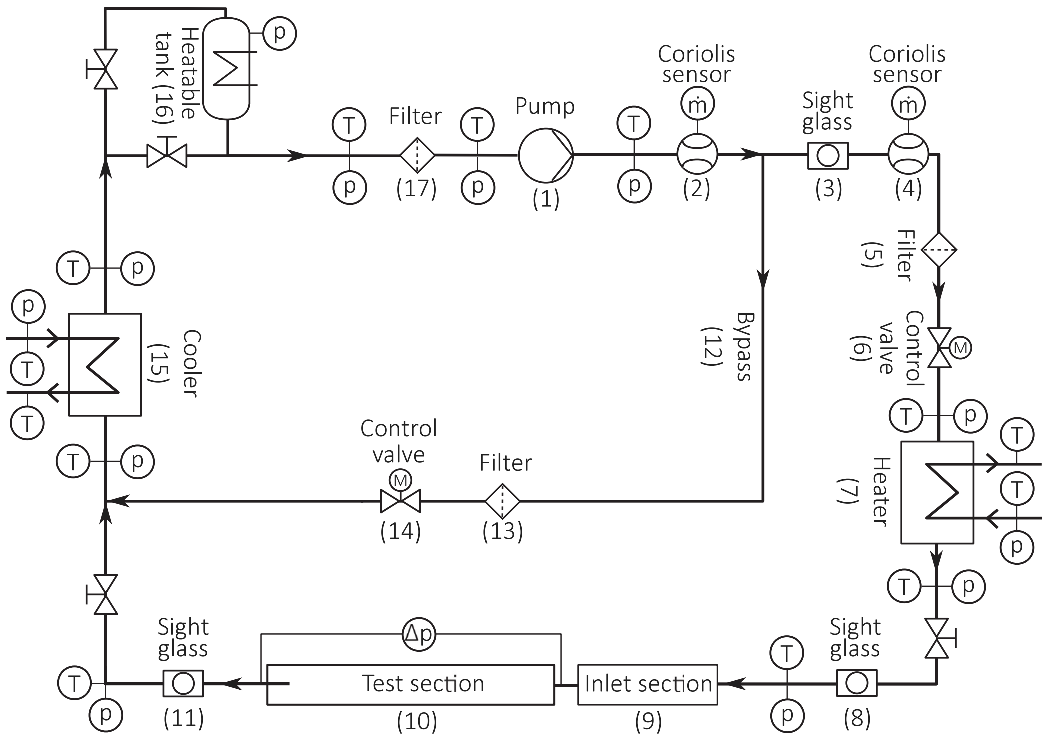

Fig. 1. Schematic of the test rig.

based on the real operating conditions of the different refrigerant line types. Fig. 1 shows a schematic of the test rig.

The process shown is based on a pump cycle. This has the advantage that no oil is needed to lubricate a compressor, so that the pure refrigerant can be examined. Furthermore, it is possible to measure all test geometries at only one installation location. The core of this process is a side channel pump (1) that circulates the liquid refrigerant. Since this type of pump requires a minimum flow rate for lubrication and cooling, part of the refrigerant must be bypassed when setting small mass flows in the test section. To measure the mass flow delivered, a first Coriolis flow sensor (2) connects to the pump, whereupon the flow splits into the main line and the bypass (12). The sight glass (3) is used to check the fluid phase, since the subsequent Coriolis sensor (4) can only accurately measure the mass flow in the main line in liquid state. A following control valve (6) is used to adjust the flow. This is done in conjunction with another control valve (14) in the bypass. In a heater PHX (7), through which hot thermal oil flows on the secondary side, the refrigerant temperature is controlled before it enters the test section. For this purpose, the temperature and the mass flow of the thermal oil are controlled. Depending on the state, liquid refrigerant is heated, partially or completely evaporated in this heat exchanger. Since this study is focused exclusively on liquid lines, the refrigerant in the experiments is only heated and not evaporated. The conditioned refrigerant flows through a sight glass (8) into an inlet section (9) which is used to calm the flow. This is followed by the interchangeable test section (10) over which the differential pressure is measured. The refrigerant then flows through another sight glass (11) and is joined with the bypass mass flow on its way to the cooler (15). Cold thermal oil flows on the secondary side of this PHX and its temperature is controlled to set the system pressure of the facility. The fluid leaves the cooler in a liquid-subcooled state and flows either directly to the suction side of the pump or through a shut-off tank with heater (16). The latter is used to shift the refrigerant from the tank to the main line when investigating liquid lines. Filters 5, 13 and 17 protect the pump and control valves from any particles.

Table 1 shows the operating range of the plant. The specified variables can be set independently of each other.

Table 1
Operating range of the system upstream of the test section.

Parameter	Range
Mass flow in $\mathrm{kg\,h^{-1}}$	30 to 300
Pressure in bar	2.5 to 24
Temperature in °C	−15 to 130

Table 2
Sensors and uncertainties.

Measured quantity	Sensor type	Range	Measurement uncertainty
Mass flow rate	Coriolis	$0\,\mathrm{kg\,h^{-1}}$ to $600\,\mathrm{kg\,h^{-1}}$	±0.1 % of m. v.
Temperature	Pt-100	−30 °C to 140 °C	±0.1 K
Pressure	Piezoresistive	0 bar to 40 bar	±0.05 bar
Pressure drop	Piezoresistive	0 bar to 3000 mbar	±3 mbar

2.1. Sensors and uncertainties

The sensors installed in the plant including their measurement uncertainties are shown in Table 2. The uncertainties of the pressure and temperature sensors result after calibration.

All analog signals from the sensors are converted into a digital signal using hardware from National Instruments and sent to a computer for analysis. The system control and data processing is done with Labview software. The pressure drop measurement starts as soon as a steady state is achieved, with data recorded at a frequency of 1 Hz over a period of 5 min. These are then time averaged in the analysis. To verify the measurement approach, a 1 m-long horizontal and straight pipe with an inner diameter of 8 mm is analyzed, and the determined resistance coefficients are compared with those calculated using the Colebrook correlation (equation (3)). The result is a mean deviation of 5.8 %, which validates the system.

3. Pressure drop analysis

A large number of empirical approaches for calculating the pressure drop of various common geometries exist in the literature. For the investigations carried out in this paper, straight pipes and bends are of particular importance. The calculation of the pressure drop is carried out using the resistance coefficient ζ, which depends on the Reynolds number:

$$\Delta p = \zeta(\mathrm{Re}) \cdot a \cdot \frac{\rho}{2} w^2 \tag{1}$$

with the Reynolds number Re

$$\mathrm{Re} = \frac{d_\mathrm{i} \rho w}{\eta}. \tag{2}$$

The factor a takes the value l/d_i for straight tubes, and 1 for other geometries. The resistance coefficient for straight tubes ζ_sp is calculated using Colebrook's equation (Colebrook, 1939):

$$\frac{1}{\sqrt{\zeta_\mathrm{sp}}} = -2 \log \left[\frac{2.51}{\mathrm{Re}\sqrt{\zeta_\mathrm{sp}}} + \frac{k/d_\mathrm{i}}{3.71} \right] \tag{3}$$

For bends of circular cross-section with $r/d_\mathrm{i} < 3$, the resistance coefficient for variable bending angles δ is obtained as (Idelčik and Ginevskiĭ, 2007):

$$\zeta_\mathrm{b} = A_1 B_1 + 0.0175\, \delta\, \zeta_\mathrm{sp} \frac{r}{d_\mathrm{i}} \tag{4}$$

Calculation of the geometry-dependent factors A_1 and B_1 can be found in the Eqs. (A.1) and (A.2) in the Appendix.

Evaluation of the measurement data is carried out with MATLAB software. The uncertainty of calculated quantities is taken into account with Gaussian error propagation. Therefore, the errors of the temperature, pressure, differential pressure and mass flow measurement are included in the uncertainty of the resistance coefficient, see Table 2. The mean relative deviation (MRD) is evaluated to assess the correlations used:

$$\mathrm{MRD} = 100\,\% \cdot \frac{1}{n} \sum \frac{x_\mathrm{calc} - x_\mathrm{meas}}{x_\mathrm{meas}} \tag{5}$$

If the MRD takes negative values, the experimentally determined quantities are correspondingly underestimated and vice versa.

A single hose, a liquid line and an underbody liquid line are analyzed in this paper. These are shielded from thermal interaction with the environment in the experiments with heat insulation, so the lines can be assumed adiabatic. All experiments are conducted with the refrigerant R1234yf at a pressure of 13 bar and a temperature of 45 °C. The subcooling in this liquid state corresponds to 5 K, the density is $1014.4\,\mathrm{kg\,m^{-3}}$, and the dynamic viscosity is 120 μPa s (Richter et al., 2011).

For the numerical investigation of the lines, in addition to one-dimensional Modelica simulations, three-dimensional CFD field simulations are also carried out with the Star-CCM+ software in version 2020.1. These involve spatial discretization of the geometry. In order to verify that the resulting polyhedral volume mesh is resolved finely enough, grid independence studies are conducted beforehand for all models. A coarse initial grid is applied and the cell size is gradually reduced until neither the pressure nor the velocity field changes. For this purpose, the fields are compared with those of the previous simulation. During the study, it was found that a finer grid is needed in the region of the pipe to hose transition pieces (TPs) than in the rest of the geometry. Especially in the wake of the TPs the velocity field is not yet formed, which is why a finer grid is applied for a better resolution of the gradients in the area from 7 mm before to 55 mm after the transition piece. Table 3 shows the mesh parameters using the single hose as an example. With two TPs the total cell count is around 19 million.

Due to the adiabatic situation and the approximate incompressibility of liquids, constant fluid properties are further assumed in the simulation. The turbulence characteristics are represented by Reynolds-averaged-Navier–Stokes model in combination with the $k-\epsilon$ model to represent the eddy viscosity. The flow boundary layer at the wall is modeled by the all-$y+$ wall treatment model. A low-$y+$ mesh is used in the TP areas where boundary layer separation is expected, and the boundary layer is thus directly resolved. A constant mass flow rate is imposed on the model at the inlet of the pipe, whereas a constant pressure is defined at the outlet. The pipes are simulated in steady state, the segregated flow solver is used as a solving algorithm.

Table 3
Mesh Parameters for the single hose.

	TP-Area	Other Areas
Average cell size in mm	0.175	0.5
Number of prism layer cells	30	2
Wall mesh	Low Y+	High Y+
Cell count in million	8.6	1.4

Table 4
Dimensions of hose section according to CAD.

Type	Length in mm	Inner diameter in mm
Straight pipe	40	7.5
Transition piece	27	5
Hose	103	8
Transition piece	27	5
Straight pipe	60	7.5

3.1. Single hose

In previous investigations, it was noticed that the results of the CFD simulation underestimated the measured values by more than 30 %. The reason for this will be explained later. Furthermore, it was found that shorter lines with two hose elements show larger pressure drops than significantly longer lines with only one hose. To clarify these discrepancies, a single hose section is first analyzed. This comes from a liquid line and is shown in Fig. 2. The geometry measured consists of two short straight pipes, two transition pieces (TP) and one hose segment. The dimensions are listed in Table 4.

The pressure drops measured in the experiment for the investigated hose section already reach up to 237 mbar at mass flow rates of $300\,\mathrm{kg\,h^{-1}}$. This leads to the conclusion that increased losses are induced within the component. Since the pipe sections and the hose are relatively short, the reason for the high pressure drops is assumed to be in the transition pieces from pipe to hose. In the following, the geometry is therefore cut open and analyzed along the main flow direction.

Fig. 3(a) shows the inside of the transition piece. This also reveals the assembly procedure. The end of the pipe is first rolled to the inner diameter of the hose so that it can be pulled over the pipe. The sealing effect against the environment is ensured by two O-rings. To prevent slippage, two grooves are rolled onto the pipe end. These are also found on the inside of the pipe in the form of two shoulders. After mounting the hose, a crimp sleeve secures the connection. The crimping process also causes another shoulder to be formed on the inside of the tube. Since the transition piece deviates greatly from the CAD drawing, a scan of the surface is made using the InfiniteFocus G4 microcoordinate measuring system from Alicona. The measured height profile is shown in Fig. 3(b) in addition to the CAD data. A significant difference between the two profiles can be recognized. While in CAD the inner diameter is abruptly reduced by 2.5 mm, the scanned profile shows a smoother transition. The shoulders caused by the crimping and the grooves can be clearly seen. It is particularly noticeable that, compared to CAD, the already reduced cross-sectional area is further decreased by the shoulders, resulting in greater hydraulic resistances. The resistance coefficient of the transition piece is determined by two different methods in the following. In the experimental approach, the pressure drops of the pipe sections and the hose calculated using equation (3) are subtracted from the measured total pressure drop of the geometry. The remaining fraction can be assigned to the transition

Fig. 2. Hose section.

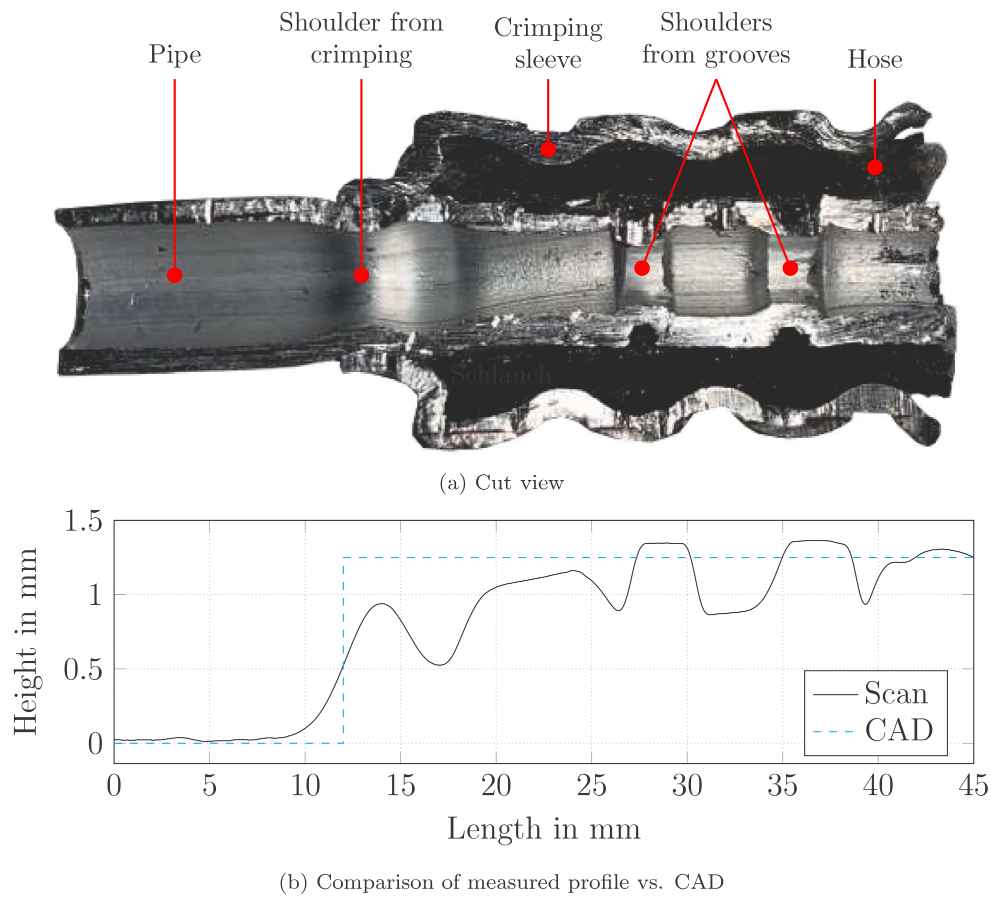

Fig. 3. Analysis of transition piece.

Fig. 4. Modified TP volume for the CFD simulation.

pieces and a resistance coefficient can be calculated for these segments. For the numerical determination of the resistance coefficient, the CAD geometry is first modified. The scanned surface profile is thereby rotated around the center axis of the pipe and thus describes the transition pieces in detail. This is shown in Fig. 4.

CFD simulations are further carried out with the improved CAD model. Finally, the resistance coefficient of the transition pieces can be determined from the calculated pressure drops. The results of the two methodologies are shown as the resistance coefficient as a function of Reynolds number in Fig. 5.

The inner diameter of the pipe of 7.5 mm is used as the reference length. It can be seen that the high-resolution simulations very accurately reflect the values obtained from the measurements. While the resistance coefficient is initially still influenced by the Reynolds number, it approaches a constant value at larger flow velocities. In order to consider the progression accordingly, this is described in the Modelica model using equation (6).

$$\zeta_{TP} = 221.7 \cdot \mathrm{Re}^{-0.555} + 6.163 \tag{6}$$

3.2. Liquid line

With the findings on the transition pieces, this section analyzes the hydraulic behavior of a liquid line connecting the condenser to the internal heat exchanger. This geometry is 1.35 m long and consists of several straight pipe sections and bends, as well as two hoses. Fig. 6 shows a picture of the line.

The investigation includes the comparison of the results of Modelica and CFD simulation with the measured values. First, the Modelica

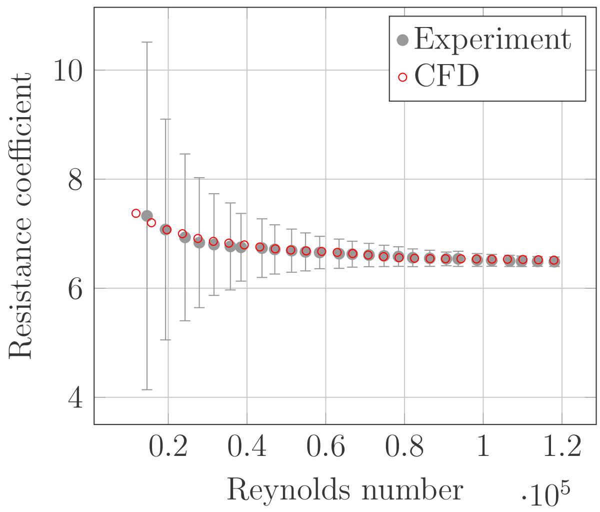

Fig. 5. Resistance coefficient of a transition piece as a function of the Reynolds number.

model is described. This consists of a serial connection of models of straight pipes and bends taken from the *AirConditioning Library* (Modelon AB, 2019). To calculate the respective resistance coefficients, Eqs. (3) and (4) are applied, where a surface roughness k of $1\,\mu\text{m}$ is used. For simplicity, the hose sections are modeled as straight pipes, while the transition pieces are modeled using equation (6). It should be noted that any flow interactions that may occur between the individual components are neglected, since usually only small bending angles or sufficiently long straight pipe sections are present. The mass flow rate and enthalpy of the refrigerant at the line inlet can be set in a flow source. After the end of the line, a sink completes the model. The Modelica model is shown in Fig. 7, the parameters of the individual model sections are shown in the Appendix in Table A.1. The solvers and GUI are provided by *Dymola* software in version 2021.

In addition, CFD simulations of the entire pipe are conducted. In this case, the original, unmodified CAD geometry is kept to show the error in using the simplified transition pieces. It should be noted that better prediction accuracy could be expected from CFD simulations of the entire pipe with modified TP geometry. However, as can be seen from Table 3, a very large discretization is already required for a single transition piece, and the resulting large number of cells would lead to very high computational time when simulating the entire pipe, so this method is not used. The simplest model is to represent the line as a straight pipe of equal length. For this purpose, equation (3) with a constant inner diameter of 7.5 mm and a length of 1.35 m is calculated and considered in the analysis. The results are shown as pressure drop as a function of mass flow rate in Fig. 8.

It can be seen that the Modelica simulations with appropriate modeling of the resistance of the transition pieces match the curve of the measured values very well and underestimate it only slightly with an MRD of −3.8 %. This is in contrast to the CFD simulation with the unmodified CAD geometry. With an MRD of −36.4 %, the measured values are significantly underestimated, with none of the simulated pressure drops falling within the ±30 % range. Modeling the line as a straight pipe of equal length is even less appropriate. In this case, the measured values are underestimated by an average of −88.7 %.

The Modelica simulations also provide information about the individual pressure loss components of the line elements. These are shown as a pie chart in Fig. 9. For the investigated liquid line with two hoses, the majority of the pressure drops are caused by the total of four transition pieces. With 84.9 %, these dominate the total pressure drop of the line, whereas the straight pipe sections and the bends with 5.5 % and 7.7 %, respectively, represent only a smaller fraction. The share of

Table 5
Charge analysis liquid line.

TP resistance	Inner diameter in mm	Pressure drop in mbar	Refrigerant charge in g
included	7.5	535	61
disregarded	7.5	81	61
disregarded	4.7	523	24
disregarded	5	386	27

the hose is also only very small with 1.9 %. Hoses generally provide mechanical decoupling of the components and can thus reduce rigid stresses or vibrations. However, for the operation of the refrigeration cycle, they mean lower efficiency due to higher pressure drops in the lines. This leads to the requirement to design the line larger, which increases the refrigerant charge, especially in the case of liquid lines.

At this point, further Modelica simulations can be carried out to investigate the hydraulic behavior of the line without the influence of the transition pieces. This could be the case, for example, if the hoses were eliminated or if an alternative pipe-to-hose connection technique were applied.

Table 5 shows the results of the investigation at a mass flow rate of $300\,\text{kg}\,\text{h}^{-1}$. The benchmark model of the real line with a total refrigerant charge of 61 g is analyzed first. The resistances of the transition pieces are considered and the internal line diameter is 7.5 mm. The total pressure drop occurring at the given mass flow is 535 mbar. In the second case, the resistance of the TPs is neglected, reducing the pressure drop of the line to 81 mbar. To show the potential of charge reduction, the diameter of the pipes is decreased. A value of 4.7 mm results in pressure drops comparable to the benchmark model of 523 mbar. In this case, the refrigerant mass is reduced by 37 g or by −61 % to a total of 24 g. Since this inner diameter does not comply with any standard size, the results for an inner diameter of 5 mm are also shown. In this case, the pressure drop is 386 mbar, and the refrigerant savings are 34 g or −56 % compared to the benchmark model.

For this section, it can be summarized that Modelica simulations have very good prediction accuracy of pressure drops if the transition pieces are modeled appropriately. Modeling the line as a straight pipe of equal length should be avoided if possible. If hoses are eliminated, there is a significant potential of charge reduction.

3.3. Underbody liquid line

In this section, an underbody liquid line is further investigated. This serves to verify the transferability of the presented method to other geometries of the same internal diameter. The analyzed line connects the internal heat exchanger to the expansion valve of a rear evaporator and has only one hose element. The total length is 2.59 m, which is significantly larger than the line studied in the previous section. Equivalent to the setup shown in Fig. 7, the Modelica model consists of a series connection of the different elements, whose parameterization can be found in Table A.2 of the Appendix. For the CFD simulations again the unmodified CAD geometry is used to illustrate the error of using a simplified model of the TPs.

Fig. 10 shows the comparison of the simulation results with the measured data. In addition, the values calculated with equation (3) for a length of 2.59 m and an inner diameter of 7.5 mm are shown. It can be seen that the Modelica simulations show very good agreement with the measured values for this line as well, overestimating them by MRD = 7.3 %. This could be due to a slightly different geometry of the transition pieces due to the manufacturing process, since even the smallest changes in the height profile change the resulting resistance due to the narrow cross-section. As with the liquid line, the pressure drops are significantly underestimated by the CFD simulation with unmodified CAD geometry with an MRD of −25.1 %. Modeling the geometry as a pipe of equal length also does not provide satisfactory results. In this case, the measured values are underestimated by −65.8 %.

Fig. 6. Investigated liquid line.

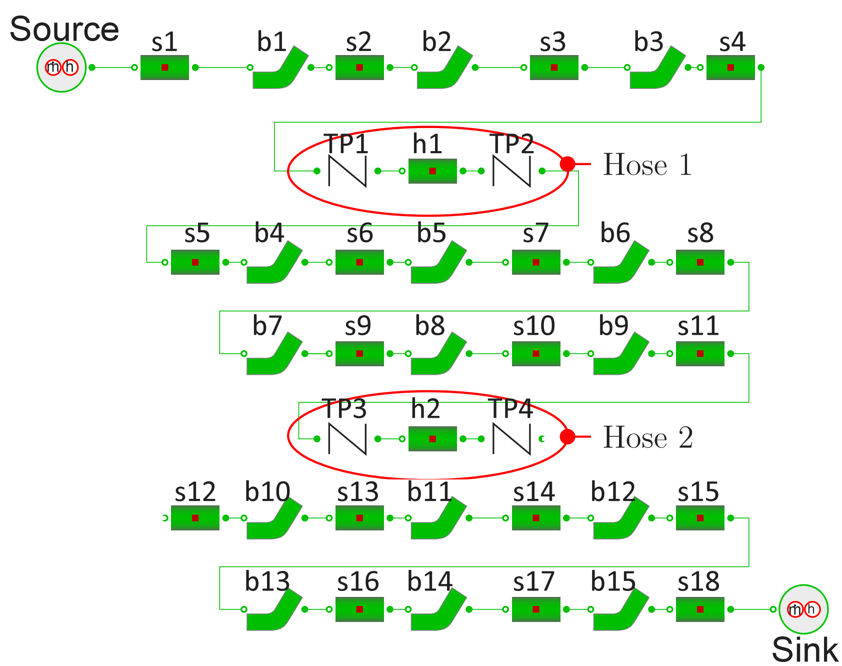

Fig. 7. Modelica model of liquid line.

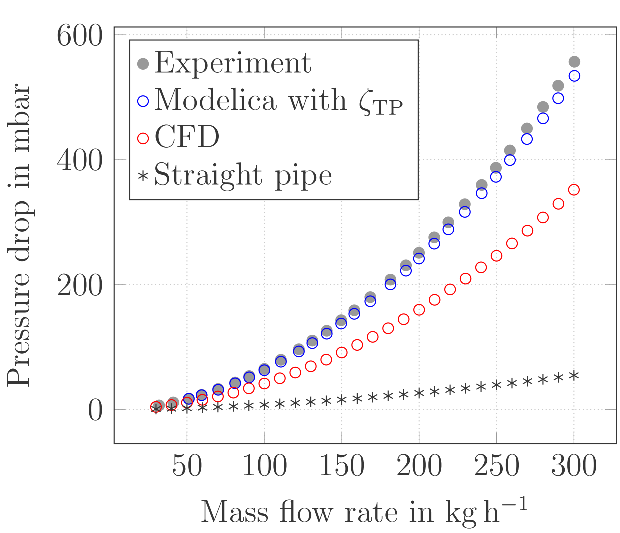

Fig. 8. Pressure drop of the liquid line as a function of mass flow rate for 13 bar and 45 °C.

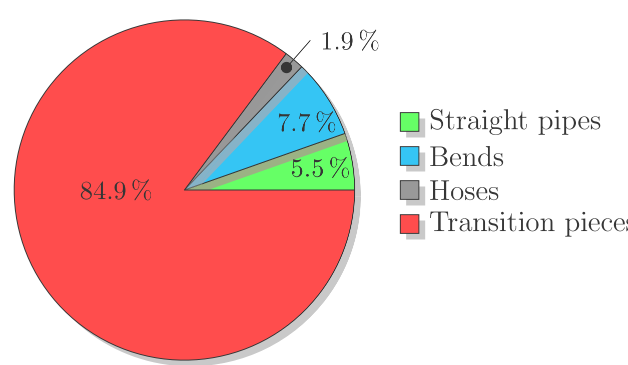

Fig. 9. Pressure drop fractions of pipe elements for the liquid line.

The distribution of the pressure drop components can be seen in Fig. 11. For the investigated geometry with only one hose element, the share of the two transition pieces is still 63.5 % of the total pressure drop. However, the fraction of the straight pipes is 25.3 %, which is significantly higher than for the liquid line with two hose elements, due to longer straight sections. The bends and the hose affect the pressure

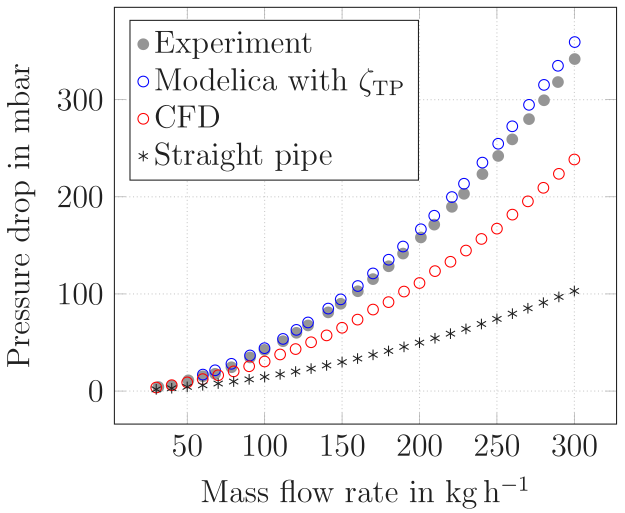

Fig. 10. Pressure drop of the underbody liquid line as a function of mass flow rate for 13 bar and 45 °C.

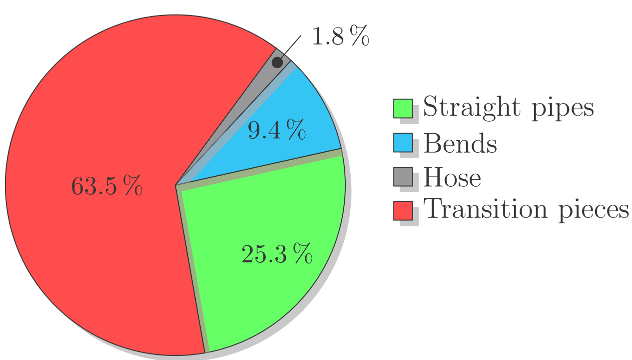

Fig. 11. Pressure drop fractions of pipe elements for the underbody liquid line.

Table 6
Charge analysis underbody liquid line.

TP resistance	Inner diameter in mm	Pressure drop in mbar	Refrigerant charge in g
included	7.5	359	116
disregarded	7.5	131	116
disregarded	5.9	360	72
disregarded	6	332	74

drop only slightly with 9.4 % and 1.8 %, respectively. Modelica simulations are also conducted for the underbody liquid line to determine the refrigerant savings when the hose element is eliminated. The results can be found for a mass flow rate of 300 kg h^{-1} in Table 6. In the benchmark model, the hydraulic resistance of the transition pieces is considered, and the resulting pressure drop is 359 mbar. Due to the long line, the refrigerant charge is 116 g, which is significantly higher than the liquid line from the previous section. When neglecting the transition pieces, the pressure drop can be reduced by −63.5 % to 131 mbar. To investigate the charge, the inner diameter is further varied. A value of 5.9 mm results in pressure drops comparable to the benchmark model at 360 mbar. In this case, the refrigerant mass is reduced by 44 g, or by −38 % to a total of 72 g. Also shown are the results for a rounded inner diameter of 6 mm. At this value, pressure drops are 332 mbar with the charge being 74 g.

For this section, it can be concluded that the Modelica simulations also provide very accurate results for the underbody liquid line. This shows that the methodology used can also be applied to other lines. Since this longer geometry has only one hose element, the influence of the transition pieces is smaller, but they still cause most of the pressure drops. By eliminating the hose, the inner diameter could be reduced to 6 mm, saving 42 g of refrigerant.

Table A.1
Dimensions of the liquid line.

No	Diameter in mm	Radius in mm	Angle in °	Length in mm
s1	7.5	–	–	20
b1	7.5	15	113	29
s2	7.5	–	–	105
b2	7.5	15	75	20
s3	7.5	–	–	20
b3	7.5	15	88	23
s4	7.5	–	–	26
b4	7.5	15	61	16
s5	7.5	–	–	14
b5	7.5	15	71	18
s6	7.5	–	–	91
b6	7.5	15	84	22
s7	7.5	–	–	23
h1	8	–	–	103
s8	7.5	–	–	37
b7	7.5	15	37	10
s9	7.5	–	–	43
b8	7.5	15	82	21
s10	7.5	–	–	37
b9	7.5	15	80	21
s11	7.5	–	–	41
b10	7.5	15	66	17
s12	7.5	–	–	56
b11	7.5	15	30	8
s13	7.5	–	–	17
b12	7.5	15	28	7
s14	7.5	–	–	16
h2	8	–	–	209
s15	7.5	–	–	14
b13	7.5	15	26	7
s16	7.5	–	–	32
b14	7.5	15	77	20
s17	7.5	–	–	15
b15	7.5	15	16	4
s18	7.5	–	–	10

4. Conclusions

In this study, the pressure drop of automotive refrigerant lines is analyzed. A test rig with the refrigerant R1234yf is available for the experimental investigation. With this, differently shaped geometries can be measured in a steady condition at different state points. The operating range of the system extends from 2.5 bar to 24 bar at pressure, −15 °C to 130 °C at temperature, and up to 300 kg h^{-1} at mass flow rate. In addition to the measurements, three-dimensional CFD simulations and one-dimensional Modelica simulations are carried out. The focus of the investigation is on liquid lines, since these offer the greatest potential for a reduction in refrigerant charge. For this purpose, a single hose is first analyzed in more detail, followed by an analysis of a liquid line and an underbody liquid line.

The main findings can be summarized as follows:

- Modeling the lines as a straight pipe of equal length is subject to a large error.
- The transition pieces from pipe to hose cause up to 85 % of the total pressure drops of the pipe in case two hoses are included.
- The determination of the resistance coefficient of the transition pieces can be done by experiments or by high-resolution CFD simulations. However, a scan of the height profile must be available for this purpose.
- With appropriate consideration of the transition pieces, very accurate predictions of the pressure drop of various pipes are possible with Modelica simulations.

Table A.2
Dimensions of the underbody liquid line.

No	Diameter in mm	Radius in mm	Angle in °	Length in mm
s1	7.5	–	–	15
b1	7.5	20	100	35
s2	7.5	–	–	41
b2	7.5	20	28	10
s3	7.5	–	–	178
b3	7.5	20	21	7
s4	7.5	–	–	67
b4	7.5	20	36	13
s5	7.5	–	–	192
b5	7.5	20	43	15
s6	7.5	–	–	150
b6	7.5	20	50	17
s7	7.5	–	–	29
h1	8	–	–	206
s8	7.5	–	–	12
b7	7.5	20	47	16
s9	7.5	–	–	16
b8	7.5	20	51	18
s10	7.5	–	–	27
b9	7.5	20	53	18
s11	7.5	–	–	76
b10	7.5	20	23	8
s12	7.5	–	–	34
b11	7.5	20	14	5
s13	7.5	–	–	45
b12	7.5	20	24	8
s14	7.5	–	–	59
b13	7.5	20	81	28
s15	7.5	–	–	111
b14	7.5	20	27	9
s16	7.5	–	–	116
b15	7.5	20	26	9
s17	7.5	–	–	377
b16	7.5	20	7	3
s18	7.5	–	–	472
b17	7.5	20	64	22
s19	7.5	–	–	46
b18	7.5	20	63	22
s20	7.5	–	–	56

Further simulations show the potential for pressure drop and refrigerant charge reduction:

- If hose elements are eliminated or an alternative connection technique is applied, the total pressure drop of the lines could be reduced accordingly by down to −85 %.
- If a comparable pressure drop as in the real line is applied, the refrigerant charge could be reduced by down to −56 % by smaller dimensioning.

Acknowledgments

The authors would like to thank TuTech Innovation GmbH, Hamburg, Germany, for their financial support for this research project.

Appendix

$$A_1(\delta) = 1.67 \times 10^{-7}\delta^3 - 8.26 \times 10^{-5}\delta^2 + 1.72 \times 10^{-2}\delta - 2.38 \times 10^{-3} \quad \text{(A.1)}$$

$$B_1(r/d_\mathrm{i}) = 0.21 \cdot \left(\sqrt{r/d_\mathrm{i}}\right)^{-0.5} \quad \text{(A.2)}$$

See Tables A.1 and A.2.

References

Cho, H., Lee, H., Park, C., 2013. Performance characteristics of an automobile air conditioning system with internal heat exchanger using refrigerant R1234yf. Appl. Therm. Eng. 61 (2), 563–569. http://dx.doi.org/10.1016/j.applthermaleng.2013.08.030.

Colebrook, C.F., 1939. Turbulent flow in pipes, with particular reference to the transition region between the smooth and rough pipe laws. J. Inst. Civ. Eng. (11.4), 133–156.

David, L.M., Barth, M., Höglund-Isaksson, L., Purohit, P., Velders, G.J.M., Glaser, S., Ravishankara, A.R., 2021. Trifluoroacetic acid deposition from emissions of HFO-1234yf in India, China, and the Middle East. Atm. Chem. Phys. 21 (19), 14833–14849. http://dx.doi.org/10.5194/acp-21-14833-2021.

Daviran, S., Kasaeian, A., Golzari, S., Mahian, O., Nasirivatan, S., Wongwises, S., 2017. A comparative study on the performance of HFO-1234yf and HFC-134a as an alternative in automotive air conditioning systems. Appl. Therm. Eng. 110, 1091–1100. http://dx.doi.org/10.1016/j.applthermaleng.2016.09.034.

Devecioğlu, A.G., Oruç, V., 2017. An analysis on the comparison of low-GWP refrigerants to alternatively use in mobile air-conditioning systems. Therm. Sci. Eng. Progr. 1, 1–5. http://dx.doi.org/10.1016/j.tsep.2017.02.002.

Di Battista, D., Cipollone, R., 2016. High efficiency air conditioning model based analysis for the automotive sector. Int. J. Refrigeration 64, 108–122. http://dx.doi.org/10.1016/j.ijrefrig.2015.12.014.

European Union, 2006. Directive 2006/40/EC of the European Parliament and of the Council of 17 May 2006 relating to emissions from air conditioning systems in motor vehicles and amending Council Directive 70/156/EEC. Off. J. Euro. Union URL http://data.europa.eu/eli/dir/2006/40/oj.

Feng, L., Hrnjak, P., 2016. Experimental and Numerical Study of a Mobile Reversible Air Conditioning-Heat Pump System. Purdue University, URL https://docs.lib.purdue.edu/iracc/1798/.

Golzari, S., Kasaeian, A., Daviran, S., Mahian, O., Wongwises, S., Sahin, A.Z., 2017. Second law analysis of an automotive air conditioning system using HFO-1234yf, an environmentally friendly refrigerant. Int. J. Refrigeration 73, 134–143. http://dx.doi.org/10.1016/j.ijrefrig.2016.09.009.

Großmann, H., 2016. Kältemittel R1234yf und CO2 im Vergleich. ATZ - Automob. Zeitschrift 118 (10), 82. http://dx.doi.org/10.1007/s35148-016-0103-4.

Huang, Y., Khajepour, A., Bagheri, F., Bahrami, M., 2017. Modelling and optimal energy-saving control of automotive air-conditioning and refrigeration systems. Proc. Inst. Mech. Eng. D 231 (3), 291–309. http://dx.doi.org/10.1177/0954407016636978.

Idelčik, I.E., Ginevskiĭ, A.S., 2007. Handbook of Hydraulic Resistance, 4., rev. and augmented ed. Begell House, Redding, Conn..

Lee, Y., Jung, D., 2012. A brief performance comparison of R1234yf and R134a in a bench tester for automobile applications. Appl. Therm. Eng. 35, 240–242. http://dx.doi.org/10.1016/j.applthermaleng.2011.09.004.

von Manstein, A., Limperich, D., Banakar, S., 2017. Simulative Comparison of Mobile Air-Conditioning Concepts for Mechanical and Electrical Driven Systems. In: Proceedings of the 12th International Modelica Conference, Prague, Czech Republic, May 15-17, 2017. In: Linköping Electronic Conference Proceedings, Linköping University Electronic Press, pp. 783–790. http://dx.doi.org/10.3384/ecp17132783.

Modelon AB, 2019. AirConditioning Library.

Navarro-Esbrí, J., Mendoza-Miranda, J.M., Mota-Babiloni, A., Barragán-Cervera, A., Belman-Flores, J.M., 2013. Experimental analysis of R1234yf as a drop-in replacement for R134a in a vapor compression system. Int. J. Refrigeration 36 (3), 870–880. http://dx.doi.org/10.1016/j.ijrefrig.2012.12.014.

Nielsen, O.J., Javadi, M.S., Sulbaek Andersen, M.P., Hurley, M.D., Wallington, T.J., Singh, R., 2007. Atmospheric chemistry of CF3CF CH2: Kinetics and mechanisms of gas-phase reactions with Cl atoms, OH radicals, and O3. Chem. Phys. Lett. 439 (1–3), 18–22. http://dx.doi.org/10.1016/j.cplett.2007.03.053.

Pabon, J.J., Khosravi, A., Belman-Flores, J.M., Machado, L., Revellin, R., 2020. Applications of refrigerant R1234yf in heating, air conditioning and refrigeration systems: A decade of researches. Int. J. Refrigeration 118, 104–113. http://dx.doi.org/10.1016/j.ijrefrig.2020.06.014.

Pottker, G., Hrnjak, P., 2015. Experimental investigation of the effect of condenser subcooling in R134a and R1234yf air-conditioning systems with and without internal heat exchanger. Int. J. Refrigeration 50, 104–113. http://dx.doi.org/10.1016/j.ijrefrig.2014.10.023.

Qi, Z., 2015. Performance improvement potentials of R1234yf mobile air conditioning system. Int. J. Refrigeration 58, 35–40. http://dx.doi.org/10.1016/j.ijrefrig.2015.03.019.

Richter, M., McLinden, M.O., Lemmon, E.W., 2011. Thermodynamic Properties of 2,3,3,3-Tetrafluoroprop-1-ene (R1234yf): Vapor Pressure and p – d – T Measurements and an Equation of State. J. Chem. Eng. Data 56 (7), 3254–3264. http://dx.doi.org/10.1021/je200369m.

Sánchez, D., Cabello, R., Llopis, R., Arauzo, I., Catalán-Gil, J., Torrella, E., 2017. Energy performance evaluation of R1234yf, R1234ze(E), R600a, R290 and R152a as low-GWP R134a alternatives. Int. J. Refrigeration 74, 269–282. http://dx.doi.org/10.1016/j.ijrefrig.2016.09.020.

Sethi, A., Hrnjak, P., 2014. Oil retention and pressure drop of R1234yf and R134a with POE ISO 32 in suction lines. HVAC&R Res. 20 (6), 703–720. http://dx.doi.org/10.1080/10789669.2014.930304.

Sharif, M.Z., Azmi, W.H., Zawawi, N.N.M., Mamat, R., Hamisa, A.H., 2020. R1234yf vs R134a in automotive air conditioning system: A comparison of the performance. IOP Conf. Ser. Mater. Sci. Eng. http://dx.doi.org/10.1088/1757-899X/863/1/012049.

Subei, C., 2020. Untersuchung des Druckverlustes und des Wärmeübergangs mit und ohne Phasenwechsel in CO2-Kältemittelleitungen (Ph.D. thesis). Hamburg University of Technology, Hamburg.

Subei, C., Schmitz, G., 2019. Analysis of refrigerant pipe pressure drop of a CO2 air conditioning unit for vehicles. Int. J. Refrigeration 106, 583–591. http://dx.doi.org/10.1016/j.ijrefrig.2019.04.005.

Xu, J., Hrnjak, P., 2018. Formation, distribution, and movement of oil droplets in the compressor plenum. Int. J. Refrigeration 93, 184–194. http://dx.doi.org/10.1016/j.ijrefrig.2018.06.020.

Zilio, C., Brown, S., Cavallini, A., 2009. Simulation of R-1234yf Performance in a Typical Automotive System, In: Proceedings of the 3rd Conference on Thermophysical Properties and Transfer Processes of Refrigeration, Boulder, CO, USA.

Zilio, C., Brown, J.S., Schiochet, G., Cavallini, A., 2011. The refrigerant R1234yf in air conditioning systems. Energy 36 (10), 6110–6120. http://dx.doi.org/10.1016/j.energy.2011.08.002.